REPORT DOCUMENTATION PAGE

Form Approved
OMB NO. 0704-0188

Public Reporting burden for this collection of information is estimated to average 1 hour per response, including the time for reviewing instructions, searching existing data sources, gathering and maintaining the data needed, and completing and reviewing the collection of information. Send comment regarding this burden estimates or any other aspect of this collection of information, including suggestions for reducing this burden, to Washington Headquarters Services, Directorate for information Operations and Reports, 1215 Jefferson Davis Highway, Suite 1204, Arlington, VA 22202-4302, and to the Office of Management and Budget, Paperwork Reduction Project (0704-0188,) Washington, DC 20503.

1. AGENCY USE ONLY (Leave Blank)	2. REPORT DATE	3. REPORT TYPE AND DATES COVERED
	May 31, 2006	Final Report, August 01, 05 – April 30, 06

4. TITLE AND SUBTITLE
Advanced Antenna Pattern Prediction Software

5. FUNDING NUMBERS
Contract FA9550-05-C-0064

6. AUTHOR(S)
Section I and 2: Thomas Jaroszewicz, Elizabeth Bleszynski, Marek Bleszynski
Section 3: Vladimir Rokhlin

7. PERFORMING ORGANIZATION NAME(S) AND ADDRESS(ES)
Monopole Research
739 Calle Sequoia, Thousand Oaks, CA 91360

8. PERFORMING ORGANIZATION REPORT NUMBER
MON- -2006-10

9. SPONSORING / MONITORING AGENCY NAME(S) AND ADDRESS(ES)

Air Force Office of Scientific Research
875 North Randolph Rd., Ste 325, Room 3112
Arlington, VA 22203
Dr Arje Nachman

10. SPO
AGE

AFRL-SR-AR-TR-06-0314

11. SUPPLEMENTARY NOTES
The views, opinions and/or findings contained in this report are those of the author(s) and should not be construed as an official Department of the Air Force position, policy or decision, unless so designated by other documentation.

12 a. DISTRIBUTION / AVAILABILITY STATEMENT

Approved for public release; distribution unlimited.

12 b. DISTRIBUTION CODE

13. ABSTRACT (Maximum 200 words)

The objective of the project was to improve performance of accurate methods for predicting radiation characteristics of antenna mounted on large platforms.

Our work concentrated mainly on an attempt of devising a viable computational scheme based on utilization of basis functions defined on large supports, and characterized by strongly collimated radiation patterns; we refer to them as "directional basis functions". The main motivation for introducing the concept of directional basis functions (in terms of specific current distributions generating such radiation patterns) is the hope that such an approach will result in a highly sparse impedance matrix which, in turn, will be amenable to the application of direct solution methods. The two main difficulties in implementing the method are (i) the relatively high cost of the directional basis functions construction and, (ii) the possible poor conditioning of the resulting set of directional basis functions stemming from their insufficient linear independence.

We implemented a numerical scheme for the construction of directional basis functions applicable to realistic surface geometries and providing near-optimal angular collimation of radiation patterns.

We carried out a detailed analysis of the origin of the ill-conditioning problem. It appears that it can be ascribed to an inherent conflict between conditioning and angular collimation; a complete set of collimated band-limited beams must involve angularly overlapping beams, and the overlap may lead to ill-conditioning. We initiated the efforts to resolve this problem.

14. SUBJECT TERMS	15. NUMBER OF PAGES
STTR report, computational electromagnetics, antenna radiation patterns, large platforms,directional basis functions, fast direct solver	IV+33
	16. PRICE CODE

20060727328

Final Report

ADVANCED ANTENNA PATTERN PREDICTION SOFTWARE

Topic # AF05-T018

Contract #: FA9550-05-C-0064

Period of Performance: 01 August 05 – 30 April, 06

Prepared by:

MONOPOLE RESEARCH
Thousand Oaks, CA 91360

with

YALE UNIVERSITY
Department of Computer Science
New Haven, CT 06520

Contents

List of Figures

1 Summary

The objective of the project was to improve efficiency of accurate methods for predicting radiation characteristics of antennas mounted on large platforms.

The computational challenge in this type of problems consists mainly of the necessity of a detailed modeling of the antenna and, at the same time, describing the much larger platform and its interaction with the antenna system. While even a complex antenna subsystem can be solved without much difficulty by the available rigorous MoM methods, computation of the antenna interaction with the platform may be out of reach of the present fast solvers, and, at the same time, asymptotic high-frequency solution techniques may not be sufficiently versatile and accurate for application to realistic problems. In addition, in problems of antenna radiation it would be highly desirable to develop efficient *direct* solution methods, which would allow predicting the radiation distribution in the entire angular range.

In this context, the goal of the present project was to make progress in developing methods alternative to the presently prevailing fast *iterative* solution techniques. Some approaches along these lines include Refs. [1, 2, 3, 4, 5, 6].

Our work was concentrated on an attempt of devising a viable computational scheme based on utilization of numerically constructed basis functions defined on large supports, and characterized by strongly collimated radiation patterns; in the following we refer to them as "directional basis functions" (DBFs). The concept of the solution scheme was to model the antenna using the conventional MoM techniques, to parameterize the platform in terms of DBFs, and to describe interactions partly iteratively (for interactions corresponding to multiple-scattering "bounces"), and partly by means of direct solution methods (for the remaining interactions, including propagation of creeping waves).

In the present project, Monopole Research concentrated on development of the DBF construction techniques, while the Yale University pursued the area of research related to direct solution methods.

The main part of our work was to implement the concept of DBFs as a mathematically precise description of well collimated beams in terms of specific current distributions generating such radiation patterns. This approach may be regarded as a rigorous realization of the concept of "rays" in high-frequency asymptotics - a mechanism not taken into account in the conventional impedance matrix compression methods. It is hoped that such an approach will result in a ***highly sparse impedance matrix*** (dominated by

couplings due to matching collimated beams radiated and received by the DBFs), which, in addition, might be amenable to the application of direct solution methods.

We stress that it appears difficult to achieve the above goals by means of constructing ***analytically*** parameterized DBFs based on asymptotic high-frequency methods, for at least two reasons: (a) the complexity and computational cost of the algorithms grows rapidly with the order of the high-frequency scattering mechanisms, and (b) in general, for a given support size, the resulting basis functions are not guaranteed to generate radiated beams of optimal angular concentration; in fact, radiation patterns generated by such basis functions tend to have high "side-lobes" (unless the behavior of the function near the boundary is regularized by using smooth partition of unity or similar, rather complex, techniques).

In this context, the principal advantages of the ***numerical*** approach to the construction of directional basis functions presented here is its relative independence of the scatterer geometry and the optimal angular collimation of the radiation patterns of the DBFs.

The main results we obtained in this effort are as follows:

- We have been able to implement a numerical scheme for construction of DBFs, applicable to realistic surface geometries, and providing, in practice, near-optimal angular collimation of radiation patterns. We confirmed that the angular widths of the pattern scale in the expected way with the support size. We illustrate the result of the algorithm on a number of cases involving realistic surface geometries (see Section 2.3).

- We found the numerical cost of DBF construction is be relatively high, and, as expected, rapidly growing with the size of the basis function support. However, on the basis of our effort under a parallel contract, where we worked on a multilevel scheme of DBF construction, we expect the cost can be reduced to the level making the procedure practical in realistic problems (see Section 2.4 for a brief description).

- We analyzed a number of scattering problems discretized by means of the constructed DBFs. We encountered here difficulties related to ill-conditioning of the impedance matrix in the DBF space resulting, essentially, from the insufficient linear independence of the DBFs. The conditioning problems seem to be of rather fundamental nature, and can be ascribed to an inherent conflict between conditioning and angular collimation, which can be summarized in a statement that

a complete set of collimated "band-limited" beams (i.e., beams generated by a spatially limited source) must involve angularly overlapping beams, and the overlap may lead to ill-conditioning.

One can also view construction of DBFs as a problem closely analogous to antenna (or antenna array) synthesis, i.e., an inherently ill-posed ***inverse scattering problem.***

In view of these difficulties, we directed a large part of the effort to the analysis of the conditioning problem:

- We carried out a detailed analysis of the origin of the ill-conditioning problems, and initiated efforts at their resolution. These efforts are discussed in Section 2.5:
  - In Section 2.5.2 we describe an attempt of modifying the operators whose eigenfunctions ("radiation modes") form a basis from which the DBFs are constructed. The modification is expected to allow us to limit the range of eigenvalues of the operators, and thus to improve conditioning of the DBF system. An interesting feature of this approach is that the operators in question describe ***spatial*** concentration of the "radiation modes", and allow construction of basis functions concentrated in both angular (essentially, Fourier) and configuration space. However, this technique requires that the supports of DBFs significantly overlap in space, which may again deteriorate conditioning. We have not yet reached a definite conclusion on the viability of the approach.
  - In Section 2.5.3 we report on an implementation of a simple iterative solution scheme, in which the DBF-space impedance matrix is used merely as a compressed matrix representation. In this approach the "near-field" part of the matrix is ***not*** discretized in terms of DBFs, which results in a significantly better conditioning.
- In the area of the development of fast direct solvers, the Yale University group designed and implemented a fast direct solver for objects in both two and three dimensions that are long and thin. An important feature of the scheme is its effectiveness in both high and low-frequency environment.

  One of the principal tools in the development of algorithms of this type is the concept of "skeletonization". It was shown that under certain

conditions (highly relevant to the design of scattering algorithms), introducing a randomized element into skeletonization schemes leads to radically improved efficiency *and* reliability.

In summary, we believe that our STTR Phase I effort contributed to the development of

- a well defined mathematical procedure for specification and numerical construction of directional basis functions,
- new efficient algorithms (with randomized elements) applicable to fast direct solution methods.

We anticipate that, as soon as the encountered difficulties are resolved, the above developments will form important building blocks for an efficient advanced antenna pattern prediction software.

2 Numerical construction of directional basis functions (DBFs) (Monopole Research report)

2.1 General features of the approach

We consider a problem of electromagnetic radiation or scattering on a perfectly conducting (closed or open) surface $\mathcal{S}$. In this case the source of radiation are the surface vector (electric) currents, tangential to the surface; we denote these sources $\mathbf{s}(\mathbf{r})$, $\mathbf{r} \in \mathcal{S}$.

The problems of acoustics and some problems of elastodynamics can be formulated by simply replacing the vector sources $\mathbf{s}(\mathbf{r})$ by scalar ones, $s(\mathbf{r})$. More general problems of elastodynamics will require using vector displacement fields.

In order to specify the problem of constructing DBFs, we construct a set of bounded connected areas $\mathcal{M}_i$ ("patches") covering the surface $\mathcal{S}$ (we may have to allow for some overlap between the patches).

Our goal is to construct, for each patch $\mathcal{M}_i$, a set of basis functions $\Psi_a^{(i)}(\mathbf{r})$, supported on the patch, which would generate a complete set of maximally collimated radiation patterns. The two requirements which would ensure an efficient numerical solution scheme are:

(i) a high angular collimation, and the resulting high impedance matrix sparsity, and

(ii) a high degree of linear independence of basis functions, and thus a reasonable conditioning of the resulting basis and of the impedance matrix in that basis.

As we indicated above, these two requirements are, to some extent, in mutual conflict: a finite patch size implies that the generated radiation patterns are band-limited in the angle (or in Fourier space); therefore, the angular distributions must have some overlapping "tails", and cannot be strictly linearly independent.

In the context of high-frequency scattering it is useful to separate the possible current distributions into a set of band-limited functions (oscillating no more rapidly than allowed by the wave number k), and the remaining ones, involving higher Fourier transforms, limited only by discretization. The class of band-limited functions is sufficient to correctly reproduce far-field interactions, and it is only this set which we attempt to represent in terms of DBFs.

In the following we give a brief overview of our approach to construction and utilization of DBFs, present the main results, and describe attempts at resolving the encountered difficulties.

2.2 Overview of the solution procedure with DBFs

In order to establish the main concepts, we give here a short description of our approach to numerical construction of the DBFs and their use in solving radiation and scattering problems.

2.2.1 DBF construction

We consider a frequency-domain radiation or scattering problem in free space, characterized by the wave number k and the wavelength $\lambda = 2\pi/k$. The asymptotic (transverse) field $\mathbf{F}_\infty$ radiated in the direction $\hat{\mathbf{q}}$ by the considered tangential vector sources $\mathbf{s}$ on a given patch $\mathcal{M} \equiv \mathcal{M}_i$ is

$$\mathbf{F}_\infty(\hat{\mathbf{q}}) = \Pi(\hat{\mathbf{q}}) \int_{\mathcal{M}} \mathrm{d}^2 r \, \mathrm{e}^{-\mathrm{i}k\,\hat{\mathbf{q}}\cdot\mathbf{r}}\, \mathbf{s}(\mathbf{r}) \;, \tag{2.1}$$

where

$$\Pi(\hat{\mathbf{q}}) = I - \hat{\mathbf{q}}\,\hat{\mathbf{q}}\;\cdot \tag{2.2}$$

projects the field onto the plane orthogonal to the radiation direction. (In the electromagnetic scattering problem with a perfectly conducting surface

the source $\mathbf{s}$ is the surface electric current, and $\mathbf{F}_\infty$ is the electric field.) The total radiated power is then

$$P = \int_{S^2} \mathrm{d}^2\hat{q}\, |\mathbf{F}_\infty(\hat{\mathbf{q}})|^2 \tag{2.3}$$

where S^2 denotes the unit two-sphere of directions $\hat{\mathbf{q}}$, and the angular integral is normalized to unity, $\int \mathrm{d}^2\hat{q} = 1$.

Similarly, we define the power radiated into a certain solid angle[1] $\Omega \subset S^2$ as

$$P(\Omega) = \int_{\Omega} \mathrm{d}^2\hat{q}\, |\mathbf{F}_\infty(\hat{\mathbf{q}})|^2 \,. \tag{2.4}$$

In terms of the sources $\mathbf{s}$ the power (2.4) can be expressed as

$$P(\Omega) = \int_{\mathcal{M}} \mathrm{d}^2r\, \mathrm{d}^2r'\, \bar{\mathbf{s}}(\mathbf{r}) \cdot h_\Omega(\mathbf{r}-\mathbf{r}')\, \mathbf{s}(\mathbf{r}') \equiv \langle \mathbf{s}\,,\, H_{\mathcal{M}}(\Omega)\, \mathbf{s} \rangle \,, \tag{2.5}$$

where the r.h.s. defines the integral operator $H_{\mathcal{M}}(\Omega)$ and the inner product $\langle \cdot\,,\, \cdot \rangle$, and where the dyadic integral kernel h_Ω is given by

$$h_\Omega(\mathbf{r}) = \int_{\Omega} \mathrm{d}^2\hat{q}\, (I - \hat{\mathbf{q}}\,\hat{\mathbf{q}}\,\cdot)\, \mathrm{e}^{\mathrm{i}k\,\hat{\mathbf{q}}\cdot\mathbf{r}} \,. \tag{2.6}$$

In the case of the total power ($\Omega = S^2$) we have

$$P = \int_{\mathcal{M}} \mathrm{d}^2r\, \mathrm{d}^2r'\, \bar{\mathbf{s}}(\mathbf{r}) \cdot h(\mathbf{r}-\mathbf{r}')\, \mathbf{s}(\mathbf{r}') \equiv \langle \mathbf{s}\,,\, H_{\mathcal{M}}\, \mathbf{s} \rangle \,, \tag{2.7}$$

with

$$h(\mathbf{r}) = \int_{S^2} \mathrm{d}^2\hat{q}\, (I - \hat{\mathbf{q}}\,\hat{\mathbf{q}}\,\cdot)\, \mathrm{e}^{\mathrm{i}k\,\hat{\mathbf{q}}\cdot\mathbf{r}} \;\equiv \frac{1}{kr}\left[1 - \mathrm{j}_1(kr)\right] + \mathrm{j}_2(kr)\, \hat{\mathbf{r}}\,\hat{\mathbf{r}}\cdot \,, \tag{2.8}$$

where the last expression (with the spherical Bessel functions j_n) is related to the imaginary part of the Green function of the usual electric-field equation. In the following we refer to the operators $H_{\mathcal{M}}(\Omega)$ and $H_{\mathcal{M}}$ as the angular

[1] An important theoretical and practical question is how to specify a reasonable set of such angles. We discuss this problem in Section 2.3.3.

and total power operators for the given surface patch $\mathcal{M}$. We assume in the following that the operators act in the space $L^2(\mathcal{M})$ of square integrable[2] tangential-vector functions $\mathbf{s}(\mathbf{r})$ on $\mathcal{M}$.

We now formulate the radiation collimation problem in terms of the Rayleigh quotient

$$\xi \equiv \xi_\Omega[\mathbf{s}] = \frac{P(\Omega)}{P} = \frac{\langle \mathbf{s}\,,\, H_{\mathcal{M}}(\Omega)\,\mathbf{s}\rangle}{\langle \mathbf{s}\,,\, H_{\mathcal{M}}\,\mathbf{s}\rangle}\ , \tag{2.9}$$

representing the fraction of the power radiated into the solid angle Ω relative to the total power. By construction,

$$0 \le \xi_\Omega[\mathbf{s}] \le 1\ . \tag{2.10}$$

The source distribution $\mathbf{s}$ generating a radiation optimally collimated within the given angle Ω is the function $\mathbf{s}$ maximizing the ratio $\xi_\Omega[\mathbf{s}]$. We construct a set of DBFs associated with the given surface patch $\mathcal{M}$ simply as a set of source (current) distributions $\mathbf{s}_a$, $a = 1, 2, \ldots$, of sufficiently high angular concentration,

$$1 - \tau \le \xi_\Omega[\mathbf{s}_a] \le 1\ , \tag{2.11}$$

where $0 < \tau \ll 1$ is an appropriately defined "power leak tolerance" (we refer to the (small) quantity $1 - \xi_\Omega[\mathbf{s}_a]$ as the power leak – the fraction of the power radiated outside the angle Ω).

Clearly, the number of solutions corresponding to angularly concentrated radiation patterns will be limited by the size of the patch, and will also depend on its shape. For sufficiently regular patches it will be of order of the Shannon number of the patch (proportional to its area in the units of the wavelength squared), i.e., to the number of linearly independent band-limited functions supported on the patch. It follows that the set of DBFs (understood as generating collimated radiation distributions) is not sufficient to represent arbitrary source distributions on the patch (limited only by discretization). The complete set of basis functions must also include current distributions weakly radiating and involving high Fourier transforms. For simplicity of notation we will denote all these functions by Ψ_a, understanding that only a part of them is associated with collimated radiation patterns.

[2]The square integrability assumption may be too weak in the case of electromagnetics, as is it known that requirements of locally finite energy of the fields usually restrict currents to smaller spaces, typically Sobolev spaces. This question requires further analysis in the present context.

Maximization of the angular concentration factor (2.9) leads (by means of functional differentiation with respect to $\bar{\mathbf{s}}$) to the stationary point condition, which has the form of the ***generalized eigenequation***

$$\int_{\mathcal{M}} \mathrm{d}^2 r'\, h_\Omega(\mathbf{r}-\mathbf{r}')\, \mathbf{s}_a(\mathbf{r}') = \xi_a \int_{\mathcal{M}} \mathrm{d}^2 r'\, h(\mathbf{r}-\mathbf{r}')\, \mathbf{s}_a(\mathbf{r}') \;, \tag{2.12a}$$

or

$$H_{\mathcal{M}}(\Omega)\, \mathbf{s}_a = \xi_a\, H_{\mathcal{M}}\, \mathbf{s}_a \;, \tag{2.12b}$$

where a labels the eigenvalues and eigenfunctions. In order to find the source distribution of the best collimated radiation pattern, we have to find the eigensolution to the highest eigenvalue ξ.

The angular collimation problem just defined belongs to the category of "concentration problems", which have been investigated by Slepian, Landau, and Pollak [7, 8, 9, 10] for band-limited functions on the real line, and later generalized to functions of several variables [11, 12, 13, 14, 15, 16, 17].

As follows from the definitions of the kernels (2.6) and (2.8), the operator $H_{\mathcal{M}}(\Omega)$ (and thus $H_{\mathcal{M}}$) is

1. self-adjoint,

$$H_{\mathcal{M}}(\Omega) = H^*_{\mathcal{M}}(\Omega) \;, \tag{2.13}$$

since

$$h_\Omega(\mathbf{r}-\mathbf{r}') = \bar{h}^{\mathrm{T}}_\Omega(\mathbf{r}'-\mathbf{r}) \;, \tag{2.14}$$

2. positive semi-definite (from Eqs. (2.4) and (2.5)), and

3. Hilbert-Schmidt (hence ***compact***), since

$$\mathrm{Tr}\left(H^*_{\mathcal{M}}(\Omega)\, H_{\mathcal{M}}(\Omega)\right) \equiv \int_{\mathcal{M}} \mathrm{d}^2 r\, \mathrm{d}^2 r'\, |h_\Omega(\mathbf{r}-\mathbf{r}')|^2 < \infty \;. \tag{2.15}$$

The above properties of the operators ensure that their spectra are discrete, non-negative, of finite degeneracy for positive eigenvalues, and with the only possible condensation point at zero.

A conventional approach to solving the generalized eigenproblem (2.12) is to first solve the eigenproblem defined by the r.h.s. operator $H_{\mathcal{M}}$, i.e.,

$$H_{\mathcal{M}}\, \mathbf{f}_\mu = \eta_\mu\, \mathbf{f}_\mu \;. \tag{2.16}$$

The spectrum is non-negative and discrete, and the eigenfunctions can be chosen orthonormal,

$$\langle \mathbf{f}_\mu \, , \, \mathbf{f}_\nu \rangle \equiv \int\limits_{\mathcal{M}} \mathrm{d}^2 r \, \overline{\mathbf{f}}_\mu(\mathbf{r}) \cdot \mathbf{f}_\nu(\mathbf{r}) = \delta_{\mu\nu} \; . \tag{2.17}$$

Physically, the eigenfunctions $\mathbf{f}_\mu$ are (square-integrable) current distributions on the patch $\mathcal{M}$, to which we refer as "radiation modes". The corresponding eigenvalues η_μ are the powers radiated by these currents,

$$\eta_\mu = \langle \mathbf{f}_\mu \, , \, H_{\mathcal{M}} \, \mathbf{f}_\mu \rangle \tag{2.18}$$

(cf. Eq.(2.7)); we assume in the following that these eigenvalues are indexed in the descending order.

By expanding the solutions $\mathbf{s}_a$ of Eq.(2.12) in terms of the eigenfunctions $\mathbf{f}_\mu$,

$$\mathbf{s}_a(\mathbf{r}) = \sum_\mu y_{\mu a} \, \mathbf{f}_\mu(\mathbf{r}) \; , \tag{2.19}$$

we obtain the discrete (matrix) eigenequation

$$\sum_\nu \langle \mathbf{f}_\mu \, , \, H_{\mathcal{M}}(\Omega) \, \mathbf{f}_\nu \rangle \, y_{\nu a} \equiv \sum_\nu h_{\mathcal{M}}(\Omega)_{\mu\nu} \, y_{\nu a} = \xi_a \, \eta_\mu \, y_{\mu a} \; . \tag{2.20}$$

By defining

$$\hat{y}_{\mu a} \equiv \sqrt{\eta_\mu} \; y_{\mu a} \tag{2.21a}$$

and

$$\hat{h}_{\mathcal{M}}(\Omega)_{\mu\nu} \equiv \frac{1}{\sqrt{\eta_\mu}} \, h_{\mathcal{M}}(\Omega)_{\mu\nu} \, \frac{1}{\sqrt{\eta_\nu}} \; , \tag{2.21b}$$

Eq.(2.20) can be brought to the conventional matrix eigenequation form

$$\sum_\nu \hat{h}_{\mathcal{M}}(\Omega)_{\mu\nu} \, \hat{y}_{\nu a} = \xi_a \, \hat{y}_{\mu a} \tag{2.22}$$

with a positive semi-definite Hermitian matrix $[\hat{h}(\Omega)_{\mu\nu}]$, and with the resulting orthonormal eigenvectors,

$$\hat{y}_a^{\mathrm{H}} \, \hat{y}_b \equiv \sum_\mu \overline{\hat{y}}_{\mu a} \, \hat{y}_{\mu b} = \delta_{ab} \tag{2.23}$$

(the superscript H denotes Hermitian conjugation). In terms of these eigenvectors, the eigensolutions of the generalized eigenequation (2.12), i.e., the DBFs, are then, finally,

$$\Psi_a(\mathbf{r}) \equiv \mathbf{s}_a(\mathbf{r}) = \sum_\mu y_{\mu a}\, \mathbf{f}_\mu(\mathbf{r}) \equiv \sum_\mu \frac{1}{\sqrt{\eta_\mu}}\, \hat{y}_{\mu a}\, \mathbf{f}_\mu(\mathbf{r}) \ . \tag{2.24}$$

The appearance of the factors $1/\sqrt{\eta_\mu}$ in this expression is of crucial importance, as it may easily cause ill-conditioning of the system of eigenfunctions $\mathbf{s}_a$. In particular, since

$$\langle \Psi_a \, , \, \Psi_b \rangle = \sum_\mu \frac{1}{\eta_\mu}\, \bar{\hat{y}}_{\mu a}\, \hat{y}_{\mu b} \ , \tag{2.25}$$

the DBFs Ψ_a would have been ***orthonormal***, were it not for the factors $1/\sqrt{\eta_\mu}$. In their presence, and if the eigenvalues η_μ span a large range, the conditioning of the set of eigenfunctions $\{\Psi_a\}$ is expected to have a larger condition number.

In fact, since the operator $H_{\mathcal{M}}$ is infinitely dimensional and compact, its spectrum must have a concentration point at $\eta = 0$. Therefore, unless we can cut off the sum over the eigenvalues at a reasonable threshold, $\eta_a \geq \eta_{\min}$, the system of DBFs may be seriously ill-conditioned. We expect similar features to persist also for the discretized, finite-dimensional operators. Therefore, we devoted a large part of work in this project to

- analyzing in more detail the origin of ill-conditioning of the DBF system, and
- investigating possible alternative formulations of the problem (in particular, modifications of the relevant operators) with the aim of improving the conditioning.

These questions are discussed in the following subsections, after we analyze the role of conditioning of the DBF system in solving scattering problems.

2.2.2 Solution of radiation and scattering problems in terms of DBFs

For definiteness and simplicity we consider electromagnetic scattering problem described by the electric-field integral equation (EFIE)[3] on the consid-

[3]However, the general solution scheme discussed here does not depend on the specific properties of the integral operator and the equation.

ered perfectly conducting surface $\mathcal{S}$,

$$\int_{\mathcal{S}} \mathrm{d}^2 r' \, G(\mathbf{r}-\mathbf{r}') \, \mathbf{J}(\mathbf{r}') = -\mathbf{E}^{\mathrm{in}}(\mathbf{r}) \;, \quad \text{for } \mathbf{r} \in \mathcal{S} \;, \tag{2.26}$$

where $\mathbf{E}^{\mathrm{in}}(\mathbf{r})$ is the incident field, and G is the Green function

$$G(\mathbf{r}) = g(\mathbf{r}) - \frac{1}{k^2} \nabla g(\mathbf{r}) \, \nabla \cdot \tag{2.27}$$

with the Helmholtz equation Green function

$$g(\mathbf{r}) = \frac{\mathrm{e}^{\mathrm{i}k\,|\mathbf{r}|}}{4\,\pi\,|\mathbf{r}|} \;. \tag{2.28}$$

In order to simplify the presentation, we do not consider the conventional MoM discretization of the above equations, but rather directly compare discretizations in terms of the sets of the orthonormal modes $\mathbf{f}_\mu$ and in terms of DBFs Ψ_a.

In the first case we represent the discretized equations in the matrix form

$$\check{A}\,\check{x} = \check{b} \tag{2.29}$$

where $\check{b}$ represents the incident field, $\check{x}$ the solution, and $\check{A}$ the impedance matrix, all having block structure associated with the patches of the surface. If Galerkin discretization is used, the current on the patch $\mathcal{M}_i$ is expanded as

$$\mathbf{J}^{(i)}(\mathbf{r}) = \sum_{\mu} \check{x}_\mu^{(i)} \, \mathbf{f}_\mu^{(i)}(\mathbf{r}) \qquad \text{for } \mathbf{r} \in \mathcal{M}_i \;, \tag{2.30}$$

elements of the vector b are projections of the incident field on the basis functions on the patch,

$$\check{b}_\mu^{(i)} = -\langle \mathbf{f}_\mu^{(i)} \,,\, \mathbf{E}^{\mathrm{in}} \rangle \equiv -\int_{\mathcal{M}_i} \mathrm{d}^2 r \, \overline{\mathbf{f}}_\mu^{(i)}(\mathbf{r}) \cdot \mathbf{E}^{\mathrm{in}}(\mathbf{r}) \;, \tag{2.31}$$

and the elements of the matrix A blocks are

$$\check{a}_{\mu\nu}^{(ij)} = \langle \mathbf{f}_\mu^{(i)} \,,\, G\,\mathbf{f}_\nu^{(j)} \rangle \equiv \int_{\mathcal{M}_i} \mathrm{d}^2 r \int_{\mathcal{M}_j} \mathrm{d}^2 r' \, \overline{\mathbf{f}}_\mu^{(i)}(\mathbf{r}) \cdot G(\mathbf{r}-\mathbf{r}') \, \mathbf{f}_\nu^{(j)}(\mathbf{r}') \;. \tag{2.32}$$

For reasonably regular patch geometries and typical MoM discretizations with spatial resolution of order 10 points per wavelength, condition numbers of the matrix blocks are moderate, say, of order 10^3 for patch size of about $4\,\lambda$.

The discretized equations in the DBF space are

$$\widehat{A}\,\widehat{x} = \widehat{b} \tag{2.33}$$

with the impedance matrix elements

$$\widehat{a}_{ab}^{(ij)} = \langle \Psi_a^{(i)}\,,\, G\,\Psi_b^{(j)} \rangle \equiv \int\limits_{\mathcal{M}_i} \mathrm{d}^2 r \int\limits_{\mathcal{M}_j} \mathrm{d}^2 r'\, \overline{\Psi}_a^{(i)}(\mathbf{r}) \cdot G(\mathbf{r}-\mathbf{r}')\, \Psi_b^{(j)}(\mathbf{r}')\,, \tag{2.34}$$

and expressions for the current and the r.h.s. analogous to Eqs. (2.30) and (2.31).

It follows from Eq.(2.24) that the DBF matrix blocks are transforms of the matrix blocks in the modes of the power operator,

$$\widehat{a}_{ab}^{(ij)} = \sum_{\mu\nu} \overline{\breve{y}}_{\mu a}^{(i)}\, \breve{a}_{\mu\nu}^{(ij)}\, \breve{y}_{\nu b}^{(j)}\,, \tag{2.35a}$$

or

$$\widehat{A}^{(ij)} = \breve{Y}^{(i)\,\mathrm{H}}\, \breve{A}^{(ij)}\, \breve{Y}^{(j)}\,, \tag{2.35b}$$

where $\breve{Y}^{(i)}$ and $\breve{Y}^{(j)}$ are transformation matrices consisting of the elements $\breve{y}^{(i)}$ and $\breve{y}^{(j)}$ for patches $\mathcal{M}_i$ and $\mathcal{M}_j$. In terms of the transformation matrix $\breve{Y}$

$$\breve{Y} = \mathrm{diag}\big[\breve{Y}^{(1)}\ \breve{Y}^{(2)}\ \ldots\ \breve{Y}^{(p)}\big] \tag{2.36}$$

(where p is the number of patches) we have then

$$\widehat{A} = \breve{Y}^{\mathrm{H}}\, \breve{A}\, \breve{Y}\,, \tag{2.37a}$$

$$\widehat{b} = \breve{Y}^{\mathrm{H}}\, \breve{b}\,, \tag{2.37b}$$

$$\breve{x} = Y\, \widehat{x}\,, \tag{2.37c}$$

i.e., we can, formally, transform the original equation (2.29) into Eq.(2.33), solve Eq.(2.33) (with a sparse matrix $\widehat{A}$), and transform the solution $\widehat{x}$ to $\breve{x}$. However, since the transformation matrix blocks may have large condition numbers (due to factors $1/\sqrt{\eta_\mu}$ in Eq.(2.24)), the transformed matrix $\widehat{A}$ blocks (in particular, the diagonal ones) may also be ill-conditioned, and solution of the system (2.33) may be practically impossible.

In Section 2.5 we address the conditioning problem in mode detail and describe our attempts at its resolution.

2.3 Construction of DBFs - numerical examples

2.3.1 Construction of eigenfunctions of the power operator

To illustrate construction of eigenfunctions of the power operator $H_{\mathcal{M}}$ for patches, we consider a curved surface patch of sizes $3\,\lambda \times 3\,\lambda$ (Fig. 1) located approximately in the (x, y) plane, and discretized with $n = 1384$ MoM unknowns (associated with the edges). The singular values σ_μ (i.e., square-roots of the eigenvalues η) of the power operator are shown in Fig. 2 (in this particular example we used the singular-value decomposition algorithm instead of the equivalent eigenvalue analysis).

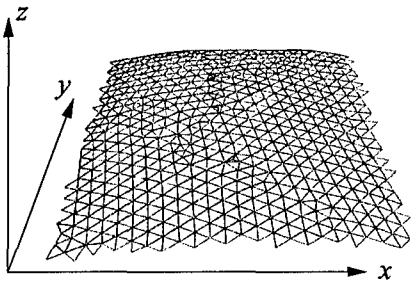

Figure 1: The surface patch $\mathcal{M}$ ($n = 1384$ MoM unknowns) used in the analysis.

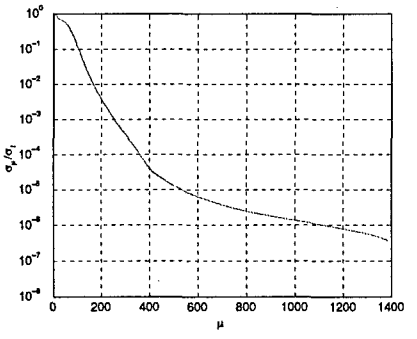

Figure 2: Distribution of the singular values of the power operator $H_{\mathcal{M}}$ of the patch of Fig. 1.

Some of the "radiating modes" (eigenfunctions of $H_{\mathcal{M}}$) are shown in Figs. 3 – 6. Figs. 3 and 4 show the current distribution and the radiation pattern for the eigenfunction associated with the highest eigenvalues η_1, and Figs. 5 and 6 the same quantities for a very weakly radiating mode with the eigenvalue $\eta_{400} \sim 10^{-10}\,\eta_1$. The radiation patterns are computed at Gauss-Legendre quadrature points on the unit sphere S^2 (for the quadrature order $L = 27$), and plotted in an approximate Mercator projection: the indices $0 \leq n_\phi < 2L$ label the quadrature points in the range $0° \leq \phi < 360°$, and the indices $0 \leq n_\theta < L$ label the quadrature points in the range $180° > \theta > 0°$ ($n_\theta = 0$ corresponds to the vicinity of the *south* pole, $\theta = 180°$).

Generally, the current distributions and radiation patterns of the strongly radiating modes are more regular than for the weakly radiating ones. A more careful analysis shows, actually, that the strongly radiating modes are of the type of standing waves. However, their radiation patterns

are practically never collimated to any appreciable degree. For example, although the radiation pattern of Fig. 4 is peaked in two approximately opposite directions ($\theta \simeq 90°$, $\phi \simeq 90°, 270°$), the level of radiation outside the peaks is not much reduced.

A characteristic feature of the weakly radiating modes is a large content of ***high Fourier transforms***, typically higher than the incident wavelength, and, near the end of the spectrum, approaching the highest oscillation rate allowed by the spatial sampling (discretization of the surface). This property is consistent with the fact the eigenfunctions associated with small eigenvalues are not band-limited.

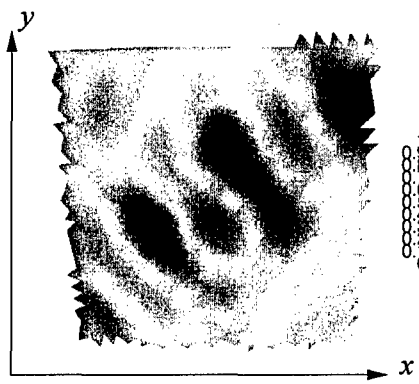

Figure 3: The real part of the y-component of the eigenfunction $\mathbf{f}_1$, corresponding to the highest eigenvalue.

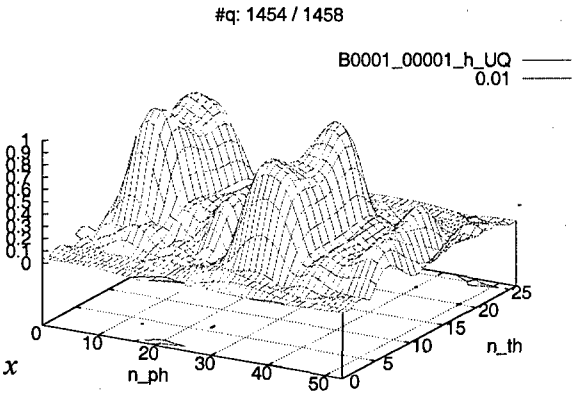

Figure 4: The radiation pattern $\widetilde{\mathbf{f}}_1$ generated by the eigenfunction of Fig. 3.

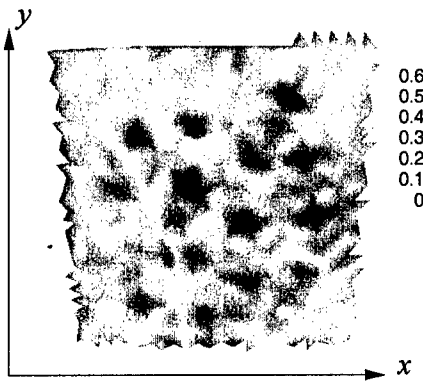

Figure 5: The real part of the y-component of the eigenfunction $\mathbf{f}_{400}$, corresponding to a small eigenvalue.

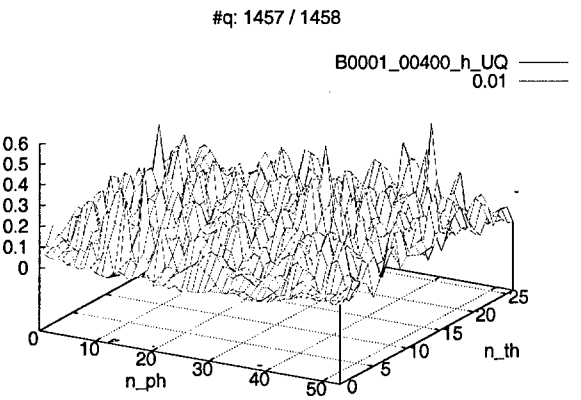

Figure 6: The radiation pattern $\widetilde{\mathbf{f}}_{400}$ generated by the eigenfunction of Fig. 5.

2.3.2 Construction of DBFs

As we described in Section 2.2.1, construction of DBFs amounts to finding angularly well concentrated solutions of the generalized eigenequation (2.12), i.e., solutions corresponding to eigenvalues close to unity.

For typical geometries, the spectrum of the eigenvalues ξ_a consists, qualitatively, of three subsets:

1. eigenvalues close to 1, i.e., solutions ***concentrated on*** Ω,
2. eigenvalues close to 0, i.e., solutions ***excluded from*** Ω, and
3. the remaining "transition eigenvalues", associated with solutions neither concentrated on, nor excluded from Ω.

The number of solutions concentrated on a given region Ω grows with the size of the region. This behavior is similar to that observed in the case of the functions concentrated on spherical cups [13, 16, 17]; however, in our problem it depends on the subsystem geometry and on the shape of the desired angular region.

The minimum angular half-width of the region (in the case the DBF is concentrated in one region only) is about $2\,\theta_{\rm N}$, where

$$\theta_{\rm N} = \frac{\lambda}{\sqrt{3}\,D} \tag{2.38}$$

is the "Nyquist angle" for a radiating system contained in a box of side D (in our example $\theta_{\rm N} \simeq 11°$). Again, however, such a statement is approximately valid only for a geometry filling more-or-less uniformly the entire box.

An important feature of the geometry-dependent radiation patterns is that in some cases, if a high concentration is to be achieved, the region Ω must consists of several disjoint areas. For example, currents on a flat surface radiate symmetrically with respect to the surface plane, and thus the region Ω must also be symmetric. A similar case is a thin, wire-like, object, for which the admissible radiation patterns must be symmetric with respect to the object axis.

We describe more details of our solution procedure in the following Section. Here we only mention that we start with a set of tentatively defined angular regions Ω and gradually expand each region until the at least one eigen-solution is sufficiently well concentrated, i.e.,

$$1 - \xi_a \leq \varepsilon\ , \tag{2.39}$$

where ε is the ***power leak tolerance***, related to the criteria of accuracy for matrix elements and for sparsity of the DBF-space impedance matrix; we typically take ε in the range 10^{-5} to 10^{-4}.

We show below some examples of DBFs constructed for the patch $\mathcal{M}$ of Fig. 1, following the procedure outlined in Section 2.2.1.

In Fig. 7 we plot distributions of the eigenvalues ξ_a for a set of six regions Ω_a, each consisting of two areas, concentrated near the poles ($\theta \simeq 0°$ and $\theta \simeq 180°$). These regions are created during the DBF construction procedure in which the initial region is being gradually expanded until the condition (2.39) is met for at least some eigen-solutions.

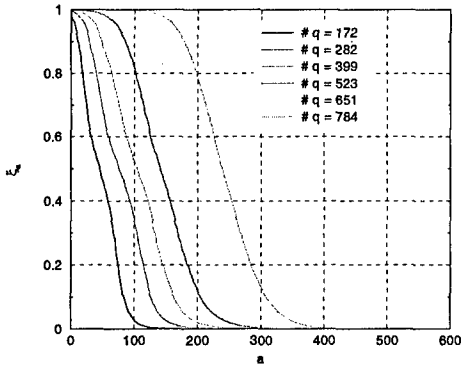

Figure 7: Distribution of the concentration factors ξ_a for a set of six angular regions Ω of increasing sizes, with the indicated numbers of directions within the region (the total number of directions is $2L^2 = 1458$).

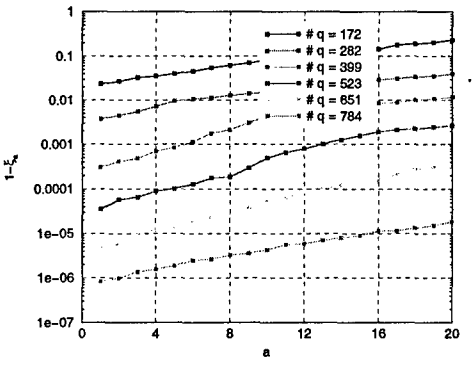

Figure 8: Distribution of the power leaks $1 - \xi_a$ corresponding to the same set of angular regions as in Fig. 7.

In the considered DBF construction our code has stopped expanding the area Ω after six steps, and selected 14 DBFs with power leaks below the assumed tolerance $\varepsilon = 10^{-5}$. The radiation patterns of the first and last of these DBFs are shown in Figs. 9 and 10.

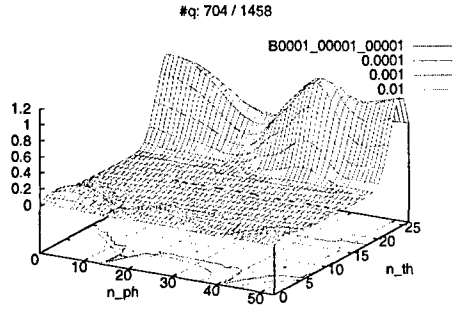

Figure 9: The radiation pattern $|\widetilde{\Psi}_1|$ of the first selected DBF for the largest angular region Ω of Fig. 7.

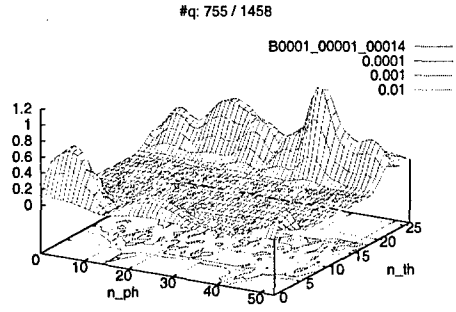

Figure 10: The radiation pattern $|\widetilde{\Psi}_{14}|$ of the last selected DBF for the largest angular region Ω of Fig. 7.

Figs. 7 and 8 show how the number of well concentrated solutions increases with the growing size of the region Ω. Typically, the minimum angular half-width of the region is about $2\,\theta_{\mathrm{N}}$, where $\theta_{\mathrm{N}} = \lambda/(\sqrt{3}\,D)$ is the "Nyquist angle" for a radiating system contained in a box of side D. In our case $\theta_{\mathrm{N}} \simeq 11°$.

However, in our example we selected the tentative angular region in the direction of the positive z-axis (the north pole). Because of the relative flatness of the considered patch (Fig. 1) it appears impossible to collimate the radiation in one direction only – here in the north-pole direction – without radiating fields in the symmetric direction. This effect is seen in Fig. 9 and especially in Fig. 10, where there is a significant radiation emitted in the direction of the south pole ($n_\theta \simeq 0$). Consequently, the selected angular region Ω is rather wide, and, finally, contains about one-half of all directions (this is partly due to the fact that the density of the quadrature points near the poles is about twice as high as near the equator).

Figs. 11 and 12 show similar results for a more favorable case of the tentative radiation direction along the x-axis ($\theta = 90°$, $\phi = 0°$). In this case it was possible to obtain a much narrower radiation pattern of the constructed DBFs. Our algorithm expanded the initial angular region in four steps, and selected, eventually, four solutions satisfying the condition (2.39).

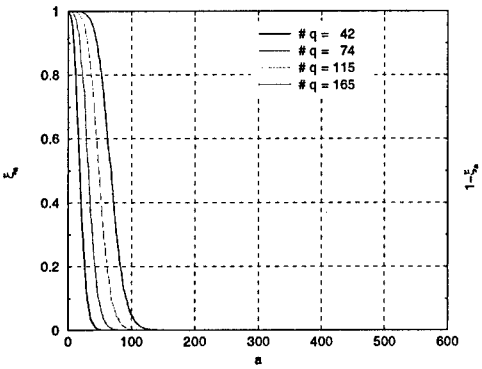

Figure 11: Distribution of the concentration factors ξ_a for a set of four angular regions Ω of increasing sizes, with the indicated numbers of directions within the region.

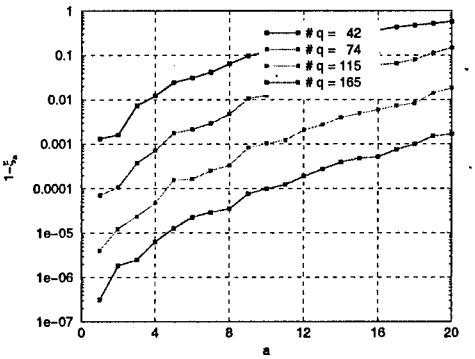

Figure 12: Distribution of the power leaks $1 - \xi_a$ corresponding to the same set of angular regions as in Fig. 11.

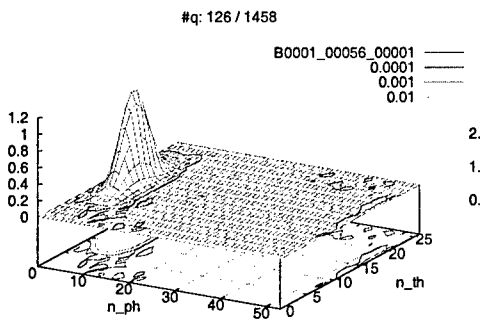

Figure 13: The radiation pattern $|\widetilde{\Psi}_1|$ of the first selected DBF for the last angular region Ω of Fig. 11.

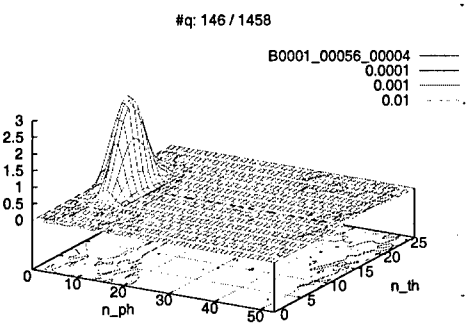

Figure 14: The radiation pattern $|\widetilde{\Psi}_4|$ of the last selected DBF for the last angular region Ω of Fig. 11.

2.3.3 Determination of angular concentration regions for DBFs

In the previous Section we showed results of constructing DBFs with radiation patterns concentrated in prescribed angular regions Ω. We now briefly

describe the procedure we use to find such regions in a way consistent with the geometry of the patch, and with the resulting physical restrictions on the admissible radiation patterns.

Our goal is to determine a given number $\mathcal{N}$ of DBFs Ψ_a concentrated with the tolerance ε (Eq.(2.39)) on as small as possible angular regions Ω_a (since the size of the regions Ω controls the sparsity of the transformed impedance matrix blocks). The number $\mathcal{N}$ of DBFs must be at least equal to the Shannon number of the patch, i.e., the approximate number of linearly independent band-limited functions (current distributions) supported on the patch; this number is

$$\mathcal{N}(\mathcal{M}) = 2\pi \frac{|\mathcal{M}|}{\lambda^2} , \tag{2.40}$$

where $|\mathcal{M}|$ is the area of the patch, and the additional factor 2 comes from the two polarizations of the electromagnetic field.

Carrying out the task of minimizing the angular regions in a rigorous way would lead to an extremely complex combinatorial problem, which would be, in practice, impossible to solve. We resort, therefore, to approximate, heuristically motivated (and based on numerical experience) methods.

We start with specifying a set of approximately uniformly distributed directions and associated regions Ω in which we would like the DBFs to radiate. We take the number of regions as

$$N_\Omega = \frac{\rho \mathcal{N}}{n_e} , \tag{2.41}$$

where $\rho \gtrsim 1$ is a "redundancy factor" and n_e is the desired average number of well-concentrated eigen-solutions per region. We adjust this number based on the considerations of numerical efficiency, since the cost of constructing more eigensolutions for a single region is lower than constructing them for separate regions; on the other hand, specifying too large regions may deteriorate angular concentration. We found that a reasonable number is of order 10.

The redundancy factor accounts for the likely possibility that (e.g., due to symmetries of the geometry) not all created DBFs will be sufficiently linearly independent; it also compensates for the unlikely cases where the DBF construction fails (i.e., no concentrated solutions are obtained for any reasonably small region Ω – see below). The number of solutions n_e depends on the size of the region, which implies that we have to choose "tentative" region sizes accordingly. An approximate value of the opening half-angle θ_Ω

of the region Ω is

$$\theta_\Omega \simeq 2\sqrt{n_e}\,\theta_N = \frac{2\sqrt{n_e}\,\lambda}{\sqrt{3}\,D}\,. \tag{2.42}$$

Having determined the set of "tentative" angular regions Ω of angular widths θ_Ω, we construct DBFs for each region Ω independently. As the first approximation, we evaluate the spherical-cap concentration function [13], say $\chi(\hat{\mathbf{q}})$, of the assumed angular width θ_Ω, concentrated on Ω. We then project that angular distribution on the space spanned by radiating modes $\mathbf{u}_\mu$. As a result, we obtain a modified angular distribution $\widehat{\chi}(\hat{\mathbf{q}})$ whose shape exhibits the features of the geometry; e.g., for a geometry with a symmetry plane, the modified distribution will have two peaks, symmetric with respect to the plane. We use the projected angular distribution to determine the updated region $\widehat{\Omega}$ as the set of directions in which the values of $\widehat{\chi}$ exceed a given threshold. We then solve the eigen-problem for the region $\widehat{\Omega}$, and, if the required concentration conditions are not met, we keep modifying (usually expanding) the region Ω until we obtain at least n_e acceptable solutions. The region Ω is being updated based on the behavior of the best concentrated solutions: we include in Ω directions in which the obtained radiation patterns exceed a threshold value.

The above procedure of finding the regions Ω usually terminates after few (typically about 5) steps, depending on the selected direction, initial size of the region, thresholds, etc. In rare cases the region Ω expands until it covers the full solid angle (or most of it). These "failed" solutions are likely to be eliminated in the stage of selecting the optimal subset of linearly independent DBFs (as described below).

In our example we constructed $N_\Omega = 134$ initial angular regions, and we obtained, on the average, 5 acceptable solutions per region, i.e., the total of 710 DBFs – about 1.3 times more than the required number. There were no "failed" construction cases, and the power leaks for the DBFs ranged from $1-\xi = 3.54\,\mathsf{e}{-8}$ to $1-\xi = 9.99\,\mathsf{e}{-6}$, with the average $1-\xi = 3.79\,\mathsf{e}{-6}$. The angular regions covered from about 8 % to 53 % of the quadrature points, with the average of 18 %.

2.4 A multilevel scheme of DBF construction

One of the practical difficulties in numerical DBF construction is its computational cost, rapidly increasing with the patch size and the number of MoM unknowns n on the patch. The main contribution to the cost, growing as n^3, is due to the eigenvalue (or singular-value) analysis. At the same time,

sufficiently large patch sizes are necessary in order to achieve an impedance compression which would would be competitive with those of more conventional matrix compression methods.

In order to alleviate this difficulty, we have investigated (within a different contract) a possibility of a hierarchical, multi-level scheme of DBF construction, in which DBFs on large patches are expressed as superpositions of DBFs on smaller sub-patches. Here we briefly summarize the main results, in order to indicate that construction of DBFs on large patches (of sizes of tens of wavelengths) may be feasible.

Our approach to the multi-level DBF construction is analogous to antenna-array synthesis, in which the array radiation pattern is a superposition of radiation patterns of its elements (DBFs of the sub-patches) with coefficients ensuring an optimal angular collimation of the array pattern. Such an optimization problem results, again, in a generalized eigenequation for the coefficients multiplying the sub-patch DBFs. In a more detailed analysis of the problem we found that a nearly optimally collimated DBF radiation into a certain solid angle Ω can be constructed by taking into account only those DBFs for sub-patches which radiate in directions overlapping the angular region Ω; this fact significantly lowers the computational cost of the construction.

As a numerical example, we present the DBF computation for a set of four adjacent level-1 patches of sizes about $3\lambda \times 3\lambda$ of a curved surface, forming a single level-2 patch of size about $6\lambda \times 6\lambda$.

Typical results are given in the Table I below. The third column gives the percentage of the solid angle covered, on the average, by the DBF radiation pattern, defined by requiring that the fraction of power radiated outside the DBF angular region is less than 10^{-4}. The total matrix compression is the product of the factor in the fourth column and an additional compression (ranging here from 0.40 to 0.10) due to elimination of a part of weakly radiating modes.

Table I
DBF collimation and construction costs

patch size	unknowns	$\|\Omega\|/4\pi$	compression	time/unknown single level	time/unknown multi-level
1.5 λ	330	45%	0.80	0.2 s	–
3.0 λ	1300	18%	0.14	2.0 s	2.0 s
6.0 λ	5200	6%	0.01	16.0 s	2.2 s

The Table shows scaling of the width of the radiation pattern of the DBF with its support size, the resulting sparsity of the far-field impedance matrix blocks, and is consistent with the computational cost of DBF construction (per unknown) approaches a constant, as expected on theoretical grounds (the total cost of constructing all DBFs should scale with the number of unknowns N as $O(N \log N)$). The times given in the Table were obtained in a computation on a single AMD Athlon processor.

Figs. 15 – 18 below visualize the behavior of a level-2 DBF constructed using all level-1 DBFs, and only the subset of the angularly overlapping DBFs.

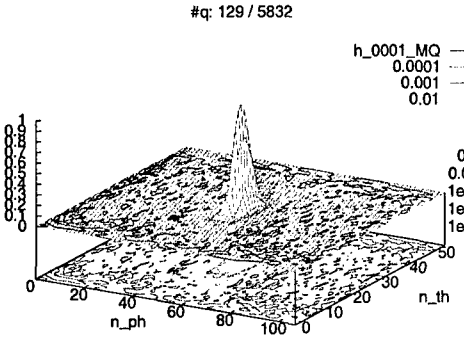

Figure 15: The radiation pattern of a level-2 DBF constructed using all level-1 DBFs.

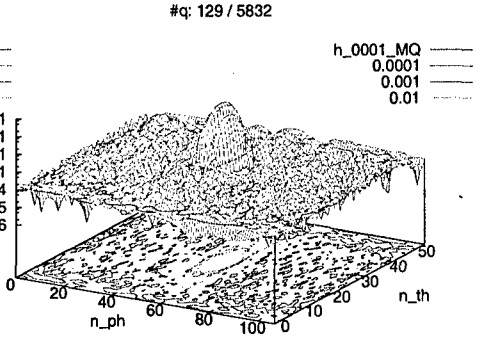

Figure 16: The radiation pattern of Fig. 15 plotted in logarithmic scale.

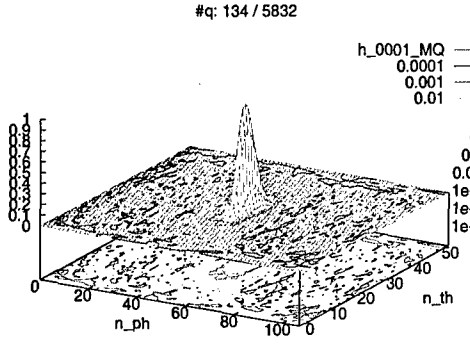

Figure 17: The radiation pattern of a level-2 DBF constructed using only a subset of overlapping level-1 DBFs.

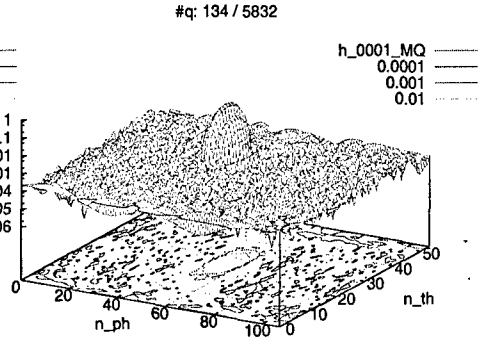

Figure 18: The radiation pattern of Fig. 17 plotted in logarithmic scale.

2.5 Analysis of the conditioning problem

We give here an account of our analysis of the ill-conditioning difficulties associated with the DBFs, and of our attempts at their resolution. We start with indicating a relation between band-limited source distributions and far-field couplings; we then proceed to discussing modifications of the power operators which lead to improved spectra of band-limited eigenfunctions, and to describing an alternative iterative solution scheme which, to large extent, circumvents the conditioning problem.

2.5.1 Computation of "far-field" matrix blocks in the DBF space

In Section 2.2.2 we expressed the matrix elements of the impedance matrix in the DBF space $\widehat{A}$ in terms of the matrix elements in the basis of the "radiation modes". Similarly, the matrix $\widehat{A}$ can be evaluated by first computing matrix blocks in the MoM basis, and then transforming them to the DBF space. However, such a procedure is computationally expensive (the cost per transformed blocks is $O(n^3)$, where n is the average number of unknowns associated with the patch).

For this reason, in the implementation of the algorithm we used an alternative expression for the DBF matrix elements, based on the Fast Multipole

Method (FMM), which allows us to compute the blocks of the matrix $\widehat{A}$ for sufficiently distant patches at a much lower cost, proportional to n^2 for patches of sizes larger than few wavelengths. We mention this algorithm at this point, since it also allows us to find upper bounds on the error in the far-field matrix elements due to possible approximations done in construction of DBFs.

We consider DBFs $\Psi_a^{(i)}$ and $\Psi_b^{(j)}$ associated with two patches, $\mathcal{M}_i$ and $\mathcal{M}_j$, such that the distance between the centers $\mathbf{c}_i$ and $\mathbf{c}_j$ of the smallest spheres enclosing the patches is larger than the sum of the radii R_i and R_j of the spheres, i.e.,

$$c_{ij} = |\mathbf{c}_{ij}| \equiv |\mathbf{c}_i - \mathbf{c}_j| > R_i + R_j \ . \tag{2.43}$$

In this case we say that the patches are, mutually, in their "far-field" range. We can then utilize the well-known Fast Multipole Method (FMM) expression for the matrix element (2.34),

$$\widehat{a}_{ab}^{(ij)} = \int\limits_{S^2} \mathrm{d}^2\,\hat{q}\ \overline{\widetilde{\Psi}}_a^{(i)}(k\,\hat{\mathbf{q}})_{\mathbf{c}_i} \cdot T(\mathbf{c}_{ij},\hat{\mathbf{q}})\,\Pi(\hat{\mathbf{q}})\,\widetilde{\Psi}_b^{(j)}(k\,\hat{\mathbf{q}})_{\mathbf{c}_j} \ , \tag{2.44}$$

where $\Pi(\hat{\mathbf{q}})$ is given by Eq.(2.1),

$$\widetilde{\Psi}_a^{(i)}(k\,\hat{\mathbf{q}})_{\mathbf{c}_i} = \int\limits_{\mathcal{M}_i} \mathrm{d}^2 r\,\mathrm{e}^{-\mathrm{i}\,k\,\hat{\mathbf{q}}\,(\mathbf{r}-\mathbf{c}_i)}\,\Psi_a^{(i)}(\mathbf{r}) \tag{2.45}$$

is the Fourier transform of the DBF $\Psi_a^{(i)}$ relative to the center $\mathbf{c}_i$ of the patch $\mathcal{M}_i$ (and similarly for the other DBF), and T is the FMM diagonal form,

$$T(\mathbf{c}_{ij},\hat{\mathbf{q}}) = \frac{\mathrm{i}k}{4\pi} \sum_{\ell=0}^{L_{\max}} (2\ell+1)\,\mathrm{i}^\ell\,\mathrm{h}_\ell^{(1)}(k\,c_{ij})\,\mathrm{P}_\ell(\hat{\mathbf{c}}_{ij}\cdot\hat{\mathbf{q}}) \ . \tag{2.46}$$

Here $\mathrm{h}_\ell^{(1)}$ is the spherical Hankel function of the first kind, P_ℓ is the Legendre polynomial, and the truncation in the angular-momentum sum is approximately $L_{\max} \gtrsim k\,(R_i + R_j)$.

The essential feature of the representation (2.44) is that the matrix element is expressed in terms of the Fourier transforms of the basis functions with the arguments not larger than k. This means that the far-field matrix elements are sensitive only to the ***band-limited components*** of the basis functions.

The above property of the representation (2.44) allows us to obtain an upper bound on the error in the DBF matrix elements due to an approximation in the DBF: if the original basis function $\Psi_a^{(i)}$ is modified to $\Psi_a^{(i)}+\Delta\Psi_a^{(i)}$, then, to the first order in $\Delta\Psi_a^{(j)}$, the variation in the matrix element is bounded by the expression

$$|\Delta\,\widehat{a}_{ab}^{(ij)}|^2 \leq M(|\mathbf{c}_{ij}|)\,P\big[\Delta\,\Psi_a^{(i)}\big]\,P\big[\Psi_b^{(j)}\big]\;, \tag{2.47}$$

where $M(|\mathbf{c}_{ij}|)$ is a function depending only on the distance between the patches, and the factors $P[\cdots]$ are total powers radiated by the current distributions $\Delta\,\Psi_a^{(i)}$ and $\Psi_b^{(j)}$, defined as in Eqs. (2.1), (2.2), and (2.3). Eq.(2.47) allows us to relate the error in the matrix elements to the eigenvalues η_μ of the radiation modes included and neglected in the computation of DBFs.

2.5.2 Alternative power operators and their spectral properties

As we discussed in Sections 2.2.1 and 2.2.2, the spectra and the eigenfunctions of the power operator $H_{\mathcal{M}}$ are the decisive factors controlling the conditioning of the constructed set of DBFs.

We have investigated possibilities of improving the conditioning by taking advantage of some arbitrariness in the definition of the angular concentration of the radiation patterns. This arbitrariness is due to the fact that, if a radiation pattern is weighted by a smooth function, it remains concentrated independently of the shape of that function (provided its variation is small over the concentration region).

We found that, by choosing appropriate weighting functions it is possible to construct such modified angular power distribution that the corresponding power operators (defined as in Section 2.2.1) have properties similar to those of the "concentration problem" operators, such as giving rise to prolate spheroidal wave functions and their generalizations, and which we encountered in the angular concentration problem. More specifically, the modified power operators define concentration of the radiation modes in space (on the patch surface).

The difference in the spectra of the original and the modified power operators is shown in Fig. 19 for a curved patch $\mathcal{M}$ of size $3\lambda \times 3\lambda$. We show the spectrum of the original operator $H_{\mathcal{M}}$ (normalized to $\eta_1 = 1$), and two modified operators denoted $H_{\mathcal{M}1}$ and $H_{\mathcal{M}2}$.

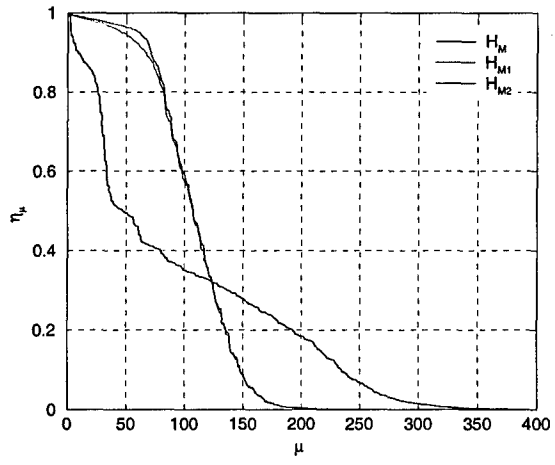

Figure 19: Spectra of the original power operator $H_{\mathcal{M}}$ and modified operators $H_{\mathcal{M}1}$ and $H_{\mathcal{M}2}$ for a patch of size $3\lambda \times 3\lambda$.

The spectra of the modified operators are similar to those of the angular concentration problem (Figs. 7 and 11): the highest eigenvalues are close to 1 (corresponding to current distributions well concentrated on the patch), and, after a transition region, the eigenvalues rapidly (exponentially) approach 0, corresponding to spatially "deconcentrated" distributions.

By using the modified power operators instead of the original ones, we are able to limit the range of the eigenvalues η_μ (since there are now more eigenvalues close to 1 in the relevant part of the spectrum); this fact improves conditioning of the DBF set. On the other hand, the spatially concentrated eigenfunctions, being band-limited, have to smoothly vanish at the patch boundaries, which requires utilizing overlapping patches, and causes deterioration of conditioning. The eventual result depends on the choice of the amount of overlap, and on the procedure of eliminating a part of the linearly dependent DBFs; we have not yet been able to find appropriate criteria ensuring reasonable DBF conditioning.

2.5.3 An alternative scattering problem solution scheme

In Section 2.2.2 we formulated the scattering problem by discretizing the integral-equation, alternatively, in terms of the "radiation modes" and in terms of DBFs. In close analogy, the conventional MoM matrix equation

$$A\,x = b \tag{2.48}$$

can be transformed to the DBF form

$$\widehat{A}\,\widehat{x} = \widehat{b} \tag{2.49}$$

(Eq.(2.33)) with

$$\widehat{A} = Y^{\mathrm{H}} A Y \,, \tag{2.50a}$$

$$\widehat{b} = Y^{\mathrm{H}} b \,, \tag{2.50b}$$

$$x = Y\,\widehat{x} \,, \tag{2.50c}$$

where Y is the transformation matrix expressing DBFs as linear combinations of the MoM basis functions.[4]

However, ill-conditioning of the system of DBFs (and thus the transformation matrix Y), causes ill-conditioning of the impedance matrix $\widehat{A}$, which may, in practice, preclude solving the problem directly (by matrix inversion). In fact, in the problems we were attempting to solve, we were not able to obtain stable solutions by means of the LU decomposition of the matrix, and even the much more expensive Singular Value Decomposition (SVD) algorithm was yielding ambiguous results.

In view of these difficulties, we implemented an alternative, iterative solution scheme, in which the DBFs are utilized only to construct a compressed representation of the impedance matrix. The procedure is as follows:

1. Separate the MoM impedance matrix into near-field and far-field blocks (associated with pairs of patches), defined according to the FMM criteria (Section 2.5.1),

   $$A = A_{\mathrm{n}} + A_{\mathrm{f}} \,. \tag{2.51}$$

   In our implementation we define patches by simply partitioning the geometry into cubic boxes. The near-field matrix block are then those coupling nearest-neighbor boxes, and the

2. Transform the far-field part of the matrix to the DBF space,

   $$\widehat{A}_{\mathrm{f}} = Y^{\mathrm{H}} A_{\mathrm{f}} Y \tag{2.52}$$

   (in the practical implementation we compute the blocks of $\widehat{A}$ directly rather than by transformation, as mentioned in the last footnote).

[4] In a practical implementation direct computation of the matrix A and its transformation would be too costly, and the transformed equation has to be constructed in a more economical way. In our implementation we compute MoM matrix blocks and transform them only in the near-field range, and evaluate the far-field matrix blocks by means of the FMM algorithm, as described in Section 2.5.1, Eq.(2.45).

3. Compute the inverse transformation matrix

$$R = Y^{-1} \tag{2.53}$$

(this matrix is also block-diagonal).

3. Solve iteratively the original equations (2.48) with the matrix A represented as

$$A = A_{\mathrm{n}} + R^{\mathrm{H}}\, \widehat{A}_{\mathrm{f}}\, R \tag{2.54}$$

and with the matrix-vector multiplication $y = A\,x$ implemented as the sequence of operations

$$y := R\,x\ , \tag{2.55a}$$
$$y := \widetilde{A}_{\mathrm{f}}\, y\ , \tag{2.55b}$$
$$y := R^{\mathrm{H}}\, y\ , \tag{2.55c}$$
$$y := A_{\mathrm{n}}\, x + y\ . \tag{2.55d}$$

Thus, the above scheme uses the DBF representation to form a compressed representation (2.54) of the original matrix A: in Eq.(2.54) A_{n} is block-sparse, R is block-diagonal, and blocks of $\widehat{A}_{\mathrm{f}}$ are sparse, provided the collimation of radiation patterns of the DBFs is sufficient.

While the procedure avoids transformation of near-field matrix blocks, there remains the problem of inverting the poorly conditioned transformation blocks Y. In practice, we found that task manageable, and were able to obtain reliable iterative solutions consistent with the original MoM solutions.

3 Developments in the formulation of fast direct solver (Yale University report)

Our work under this contract can be roughly subdivided into two parts: development of tools specific to the problems to be addressed, and the work involving collateral issues. As often happens, in a number of cases collateral issues had to be addressed in order to deal effectively with the principal subject of research. Below is a brief discussion of both types of issues addressed by the project.

In addition to these investigations, we have been reporting results obtained recently (but prior to the start of the current contract). These can be found in [21], [22], [23],

1. We designed and implemented a fast direct solver for objects in both two and three dimensions that are long and thin. This work involved the "fast" element of the algorithm, the rapidly convergent discretizations in various situations, and the required asymptotic analysis. An important feature of the scheme is its effectiveness in both high and low-frequency environment. This work has been reported in [18]; the scheme has been generalized to two dimensions, and the algorithm is being implemented.

2. One of spin-offs of this activity is an observation that given a set of n very general bounded functions $\varphi_1, \varphi_2, \ldots, \varphi_n$ (with a finite n), there exist stable n-point interpolation and quadrature formulae exact on the linear space spanned by the functions $\varphi_1, \varphi_2, \ldots, \varphi_n$. This is a somewhat unexpected observation, and its proof depends entirely on linear algebraic arguments; we have also implemented numerical algorithms for the construction of such interpolation and quadrature formulae applicable in many situations of practical interest (in addition to the uses of such schemes in numerical scattering theory). These results are reported in [19].

3. One of the principal tools in the development of algorithms of this type is the concept of "skeletonization" (see, for example, [22]). Recently, it turned out that under certain conditions (highly relevant to the design of scattering algorithms), introducing a randomized element into skeletonization schemes leads to radically improved efficiency *and* reliability. These results are reported in [20]).

References

[1] R. J. Burkholder and D.-H. Kwon, "High-frequency asymptotic acceleration of the fast multipole method," *Radio Science*, vol. 31, pp. 1199–1206, 1996.

[2] V. V. S. Prakash and R. Mittra, "Characteristic basis function method: a new technique for efficient solution of method of moments equations," *Microwave and Optical Technology Letters*, vol. 36, pp. 95–100, 2003.

[3] R. Mittra and V. V. S. Prakash, "The characteristic basis function method: a new technique for solution of radar scattering problems," *CMES*, vol. 5, pp. 435–442, 2004.

[4] L. Matekovits, G. Vecchi, G. Dasano, and M. Orefice, "Synthetic functions analysis of large printed structures: the solution space sampling approach," in *Proceedings of the 2001 IEEE AP-S International Symposium*, July 3-13, 2001, pp. 568–571.

[5] F. X. Canning and K. Rogovin, "Simply sparse, a general compression/solution method for mom programs," in *2002 IEEE Antennas and Propagation International Symposium*, San Antonio, TX, 2002, April 3-7, 2002, pp. 234–237.

[6] F. Canning, "Creating directional beams from numerical data," in *2005 IEEE AP-S Symposium and USNC/URSI National Radio Science Meeting*, Washington, DC, 2005, July 3-8, 2005.

[7] D. Slepian and H. O. Pollak, "Prolate spheroidal wave functions, Fourier analysis and uncertainty – I: The dimension of the space of essentially time- and band-limited signals," *Bell Syst. Tech. J.*, vol. 40, pp. 43–63, 1960.

[8] H. J. Landau and H. O. Pollak, "Prolate spheroidal wave functions, Fourier analysis and uncertainty – II," *Bell Syst. Tech. J.*, vol. 40, pp. 65–84, 1960.

[9] H. J. Landau and H. O. Pollak, "Prolate spheroidal wave functions, Fourier analysis and uncertainty – III: The dimension of the space of essentially time- and band-limited signals," *Bell Syst. Tech. J.*, vol. 41, pp. 1295–1336, 1962.

[10] D. Slepian, "Some comments on Fourier-analysis, uncertainty and modeling," *SIAM Rev.*, vol. 25, pp. 379–393, 1983.

[11] D. Slepian, "Prolate spheroidal wave functions, Fourier analysis and uncertainty – IV: Extensions to many dimensions; generalized prolate spheroidal wave function," *Bell Syst. Tech. J.*, vol. 41, pp. 1295–1336, 1962.

[12] E. N. Gilbert and D. Slepian, "Doubly orthogonal concentrated polynomials," *SIAM J. Math. Anal.*, vol. 8, pp. 290–319, 1977.

[13] F. A. Grünbaum, L. Longhi, and M. Perlstadt, "Differential operators commuting with finite convolution integral operators: some non-abelian examples," *SIAM J. Appl. Math.*, vol. 42, pp. 941–955, 1982.

[14] A. Albertella, F. Sansò, and N. Sneeuw, "Band-limited functions on a bounded spherical domain: the Slepian problem on the sphere," *J. Geodesy*, vol. 73, pp. 436–447, 1999.

[15] L. Miranian, "Slepian functions on the sphere, generalized Gaussian quadrature rule," *Inv. Prob.*, vol. 20, pp. 877–892, 2004.

[16] M. A. Wieczorek and F. J. Simons, "Localized spectral analysis on the sphere," *Geophys. J. Int.*, vol. 160, pp. 1–24, 2005.

[17] F. J. Simons, F. A. Dahlen, and M. A. Wieczorek, "Spatiospectral concentration on a sphere," *SIAM Rev.*, vol. to be published, 2005.

[18] P.G. Martinsson and V. Rokhlin, "A fast direct solver for scattering problems involving elongated structures," YALEU/DCS/RR-1347, 2006, to appear in *Journal of Computational Physics.*

[19] P.G. Martinsson, V. Rokhlin, and M. Tygert, "On interpolation and integration in finite-dimensional spaces of bounded functions," YALEU/DCS/RR-1353, 2006, to appear in Communications in Applied Mathematics and Computational Science (CAMCoS).

[20] P.G. Martinsson, V. Rokhlin, and M. Tygert, "A randomized algorithm for the approximation of linear operators," YALEU/DCS/RR-1352, 2006.

[21] V. Rokhlin and M. Tygert, "Fast algorithms for spherical harmonic expansions," SIAM J. Sci. Comput. , 27(6): 1903-1928, 2006.

[22] P.G. Martinsson and V. Rokhlin, A Fast Direct Solver for Boundary Integral Equations in Two Dimensions, *Journal of Computational Physics*, 205 (2005), pp. 1-23.

[23] P.G. Martinsson and V. Rokhlin, An Accelerated Kernel-Independent Fast Multipole Method in One Dimension, YALEU/DCS/RR-1353, 2006.